Electronic Supplementary Material (ESI) for Physical Chemistry Chemical Physics.
This journal is © the Owner Societies 2017

Biomembrane Solubilization Mechanism by Triton X-100: A Computational Study of The Three Stage Model

Antonio Pizzirusso[a], Antonio De Nicola[a,], G. J. Agur Sevink[b], Andrea Correa[c], Michele Cascella[d], ToshihiroKawakatsu[e], Mattia Rocco[f], Ying Zhao[g], Massimo Celino[h], Giuseppe Milano[a,]**

[a] Dipartimento di Chimica e Biologia, Università di Salerno, Via Giovanni Paolo II, 132, I-84084, Fisciano, Italy.
[b] Leiden institute of Chemistry, Leiden University, P. O. Box 9502, 2300 RA Leiden, The Netherlands.
[c] Department od Chemical Science, Federico II University of Naples, Via Cinthia, Complesso Monte S. Angelo, 80126 Naples, Italy.
[d] Department of Chemistrya and Hylleraas Centre for Quantum Molecular Sciences, University of Oslo, Sem Sælandsvei 26, 0371 Oslo, Norway.
[e]Department of Physics, Tohoku University, Aoba, Aramaki, Aoba-ku, Sendai 980-8578, Japan.
[f]Biopolimeri e Proteomica, Ospedale Policlinico San Martino, Largo R. Benzi 10, I-16132 Genova, Italy.
[g]Institute of Nano-Photonics, School of Physics and Materials Engineering, Dalian Minzu University, Dalian 116600, China
[h]ENEA, C.R. Casaccia, Via Anguillarese 301, I-00123 Roma, Italy.

* corresponding authors: gmilano@unisa.it, adenicola@unisa.it

Electronic Supporting Information

Systems Compositions

Table S1

	TX-100/DPPC	No. of Particles	DPPC	Water	TX-100	System	Density (kg/m^3)	Box Size (nm^3)	Time (μs)
	Bilayers								
I	0.43 (U)	75000	875	59250	375	PP	1120.03	16.82x16.82x26.95	7.3
II	0.43 (S)	75000	875	59250	375	PP	1033.68	18.94x18.94x23.03	6.5
III	1.0 (U)	75000	625	58750	625	PP	1057.56	14.93x14.93x35.78	6.3
IV	1.0 (S)	75000	625	58750	625	PP	1137.22	16.88x16.88x26.03	6.3
V	0.43 (U)	75375	875	59250	375	PF	1120.03	16.82x16.82x26.95	7.4
VI	0.43 (S)	75375	875	59250	375	PF	1033.68	18.94x18.94x23.03	7.7
VII	1.0 (U)	75625	625	58750	625	PF	1057.56	14.93x14.93x35.78	5.7
VIII	1.0 (S)	75625	625	58750	625	PF	1137.22	16.88x16.88x26.03	5.7
IX	0.43 (S)	301500	3500	237000	1500	PF	1120.03	33.64x33.64x26.95	3.0
X	0.43 (U)	301500	3500	237000	1500	PF	1033.68	37.88x37.88x23.03	6.8
XI	1.0 (U)	302500	2500	235000	2500	PF	1057.56	29.86x29.86x35.78	4.7
XII	1.0 (S)	302500	2500	235000	2500	PF	1137.22	33.76x33.76x26.03	5.2
XIII	10.0 (S)	302500	450	235000	4550	PF	1057.56	33.76x33.76x26.03	3.8
	Vesicles								
XIV	0.10 (W)	195524	877	183680	88	PF	1053.26	28x28x28	4.5
XV	0.43 (W)	195524	877	179345	377	PF	1043.31	28x28x28	5.7
XVI	1.0 (W)	195524	877	171845	877	PF	1026.10	28x28x28	4.5
XVII	0.10 (S)	195524	797	184760	80	PF	1054.32	28x28x28	4.5
XVIII	0.10 (I)	195524	797	184760	80	PF	1054.32	28x28x28	4.8
XIX	0.10 (O)	195524	797	184760	80	PF	1054.32	28x28x28	4.8
XX	0.43 (S)	195524	613	184208	264	PF	1049.80	28x28x28	4.5
XXI	0.43 (I)	195524	613	184208	264	PF	1049.80	28x28x28	4.8
XXII	0.43 (O)	195524	613	184208	264	PF	1049.80	28x28x28	4.8
XXIII	1.0 (S)	195524	439	183686	438	PF	1045.52	28x28x28	4.5
XXIV	1.0(I)	195524	439	183686	438	PF	1045.52	28x28x28	4.8
XXV	1.0(O)	195524	439	183686	438	PF	1045.52	28x28x28	4.8
XXVI	10.0 (S)	196604	79	183686	798	PF	1042.55	28x28x28	6.0
XXVII	0.0	195524	877	185000	0	PF	1056.29	28x28x28	3.3
XXVIII	0.43(S)	569000	4055	494765	1745	PF	1048.99	40x40x40	4.5 ns

Particle-Field CG Model Parameters

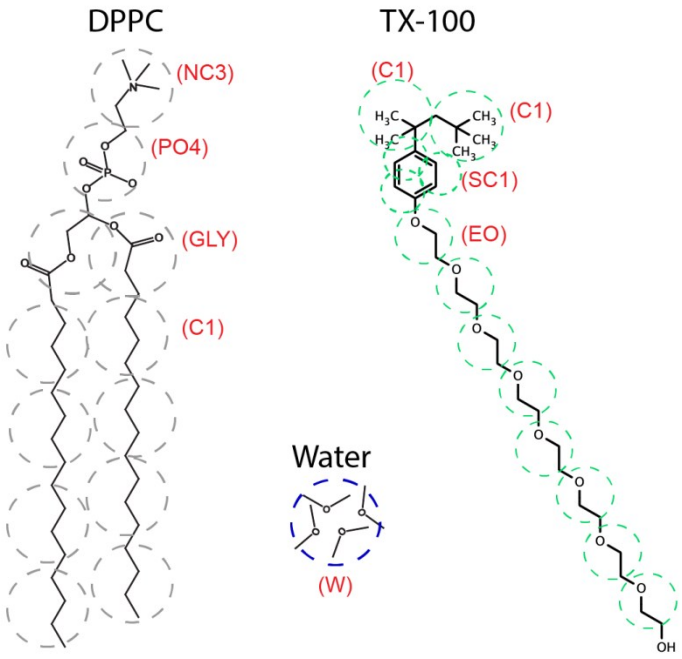

Figure S1: Mapping scheme adopted for PP and PF CG models. Next to each atom group is reported the corresponding label of CG effective particle type.

The mapping scheme of the CG Particle-Field (PF) models, for DPPC, water and TX-100molecules, is reported in Figure S1. The heavy atoms of effective CG bead types are grouped and identified by segmented circles. Next to each bead type is reported the corresponding label.

In the PF model the bonds are described by a harmonic potential having the functional form:

$$V_{bond}(l) = \frac{1}{2} K_{bond}(l - l_0)^2, \qquad \text{(S1)}$$

where l_0 is the equilibrium distance and K_{bond} is the force constant of the bond.

In Table S2 are reported the l_0 and K_{bond} parameters used for the PF models, while the set of parameters of the Particle-Particle (PP) reference models, based on the Martini force-field, can be found in references[1-3].

Table S2. Bond Interaction Parameters for the CG model of TX-100

Bond	l_0 (nm)	K_{bond} (kJ/mol nm^2)
C1-C1*	0.37	1250
C1-SC1	0.27	7500
SC1-SC1	0.27	8000
SC1-EO	0.28	5000
EO-EO	0.28	8000
NC3-PO4	0.47	1250
PO4-GLY	0.47	1250
GLY-GLY	0.37	1250
GLY-C1	0.47	1250

* For the DPPC molecule the bond length is 0.47 nm

The angles θ between two successive bonds is described by a harmonic potential $V_{angle}(\theta)$ depending of the cosine of θ. The functional form of the harmonic potential, together with a list of the force constants K_{angle} and equilibrium bond angles θ_0 are reported in the Table below.

$$V_{angle}(\theta) = \frac{1}{2}K_{angle}\{cos(\theta) - cos(\theta_0)\}^2, \quad \text{(S2)}$$

Table S3. Angle Interaction Parameters for the CG model of TX-100

Angle	θ_0 (deg)	K_{angle} (kJ/mol)	**Angle**	θ_0 (deg)	K_{angle} (kJ/mol)
C1-C1-SC1	140	30	EO-EO-EO	155	40
C1-SC1-SC1	140	30	PO4-GLYGLY	120	25
SC1-SC1-SC1	120	40	PO4-GLY-C1	180	25
SC1-SC1-EO	140	30	GLY-C1-C1	180	25
SC1-EO-EO	155	40	C1-C1-C1	180	25

The Particle-Field interactions parameters $\chi_{KK'}$ need to be fixed for every type of non-bonded interaction between a particle K-type and the density field obtained from the particles of type K'. In Table S4 are reported the $\chi_{KK'}$ interaction parameters of PF models used in the present study.

Table S4. Mean-field parameters $\chi_{K,K''}$×*RT* (kJ/mol) for the interaction of a particle of type *K* with the density fields due to particles of type *K'* used in eq. 2 of main text.

Bead Type	**NC3**	**PO4**	**GLY**	**C1**	**SC1**	**EO**	**W**
NC3	0.0	-1.5	6.3	9.0	9.0	-5.25	-8.1
PO4		0.0	4.5	13.35	13.5	-0.75	-3.6
GLY			0.0	6.3	6.3	5.0	4.5
C1				0.0	2.4	7.8	33.75
SC1					0.0	7.8	20.25
EO						0.0	1.5
W							0.0

For a vesicle with intermediate radius of curvature, all simulation parameters are the same as before, apart from the following: the field discretisation (l = 0.5 nm), the field update frequency (every 5th time step), and the time step (dt = 0.01 ps). In particular, we used rather conservative values for these linked parameters, because we found that the initial process of deflation is rather slow for the original field update frequency, which may bias the vesicle evolution.

Systems Construction.

We chose to build initial systems by considering two aspects: first, the TX-100/DPPC ratio R and, second, the curvature of the lipid bilayer. According to the experimental R_e^{sat} and R_e^{sol} limits obtained[4] at T = 299 K, we selected three different R values, below (R = 0.1), close to the saturation limit (R = 0.43), and equal to the solubilization limit (R = 1.0). The TX-100/DPPC ratio is not the only parameter that controls the solubilization. TX-100 interacts with DPPC bilayers also depending on the physical state of the lipid (gel or fluid), that in turns depends on the temperature.[4,5] In particular, the gel-fluid transition temperature (Tm) of DPPC, experimentally observed at 314 K, is also influenced by the TX-100 concentration; in fact, increasing the amount of TX-100, the Tm of DPPC decreases by a few degrees.[6] From the simulation point of view, the gel-liquid transition temperature is usually shifted to lower values when CG models are employed for molecular simulations. For instance, the MARTINI model for the DPPC bilayer shows a liquid to gel transition is lower of about 20 K, and even pure DPPC models are already fluid[1] at 298 K. Moreover the presence of TX-100, according to experimental observations, confirms a further decrease in transition temperature, as reported in our recent publication.[3] Finally, the hybrid Particle-Continuum formulation of the models employed in the present study does not show any gel phase for pure DPPC and the simulation are all carried out in the fluid phase, even if the gel phase is observed at 298 K. It is worth to note that the membrane remains insoluble in the gel phase only at very low temperatures, and for temperature values higher than 296 K DPPC becomes solubilized by TX-100 showing R_e^{sat} and R_e^{sol} comparable to those in the fluid phase.[4] For this reason, we decided to compare our simulation results in relation to TX-100/DPPC ratios. We considered this a reasonable choice that connects the good properties of TX-100 as a detergent in the fluid phase, and the comparison of the available data at a given temperature.

A second important aspect we have considered in the systems building is the curvature of the bilayer. In particular, systems were built with finite curvature (spherical vesicle) and in the infinite limit curvature radius (flat bilayer surface). Moreover, the TX-100 molecules were distributed in the lipid bilayer in two ways: i) symmetrically, in which all TX-100 molecules are equally and randomly distributed between both membrane layers, ii) asymmetrically, in which all TX-100 molecules are randomly distributed inside only one layer of the membrane bilayer. In Scheme S1, simplified representations of symmetric and asymmetric configurations, for flat and curved bilayer surfaces, are reported. The systems with flat surface (infinite curvature limit) are labelled with U and S. The first indicates an asymmetric TX-100 distribution, while the second indicates a symmetric TX-100 distribution. According to the generalisation of the original Three Stage Model mechanism proposed by Lichtenberg,[7] consisting in the fast and slow repartition of the detergents (Scheme 1 of the main manuscript), we decided to build two different types of initial configurations for flat bilayer systems, corresponding to two limiting cases. In the first case, a symmetric distribution of the TX-100 molecules represents a case where the uptake process of TX-100 from solution into the membrane can be considered slower that TX-100 flip-flop (labelled with S, fast repartition of the detergent). The other case, where the detergent molecules are asymmetrically located only in the upper layer, represents a case where the uptake process of TX-100 can be considered instead faster than TX-100 flip flop (labelled with U, slow repartition of the detergent).

For the vesicle simulation, coordinates of DPPC vesicle composed of 877 molecules were downloaded from the Marrink GC web site

(http://md.chem.rug.nl/;marrink/MARTINI/Coordinates.html).

The pure DPPC vesicle is then equilibrated by using the Particle-field approach. In Figure S2 we report the percentage of molecules in the inner and the outer layers as functions of the simulation

time, confirming that the vesicle is created without stress destabilizing it. In fact, these percentages remain constant during the simulation time.

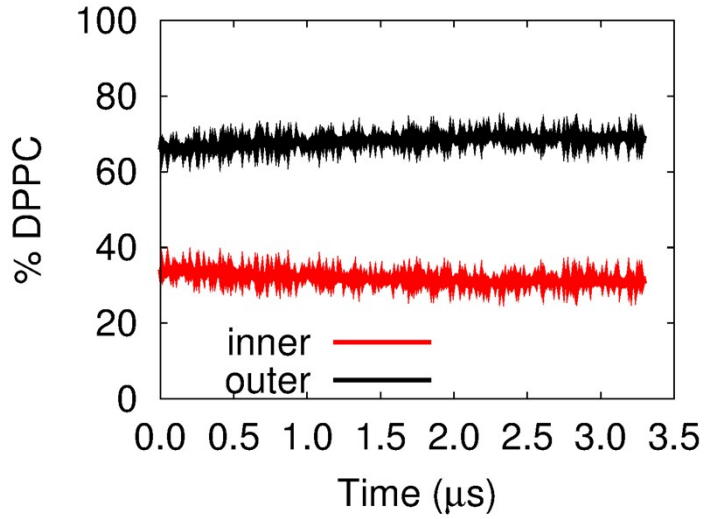

Figure S2: Percentage of DPPC molecule in the inner (red) and outer (black) layers as function of simulation time for a pure DPPC vesicle.

Part of the lipids are then randomly converted from DPPC to TX-100 in order to obtain the TX-100/DPPC ratios of 0.1, 0.43 and 1.0, respectively. These configurations are inserted in a cubic box of 28×28×28 nm, and water molecules are added both to the cavity, where a density of 9 water molecules in 1 nm^3 was employed, and outside the vesicle, providing an appropriate value of the overall system density. More details about these systems are summarized in Table S1. The systems with finite curvature radius (spherical vesicles) are labelled with S, O, I and W. The label W indicates that TX-100 is initially distributed in the water phase, while the label S indicates a symmetric distribution of TX-100 between the inner and outer layer of a vesicle. With the labels O and I we refer to an asymmetric distribution of TX-100 in the outer and inner layers of a vesicle, respectively. Combining the different TX-100 concentrations with the symmetric and asymmetric TX-100 initial distributions, twenty-three different initial systems were built. In Table S1, the composition of each simulated system is reported. The area/molecule ratio of the TX-100/DPPC mixed bilayer is equal to that reported by Pizzirusso et al.[3]

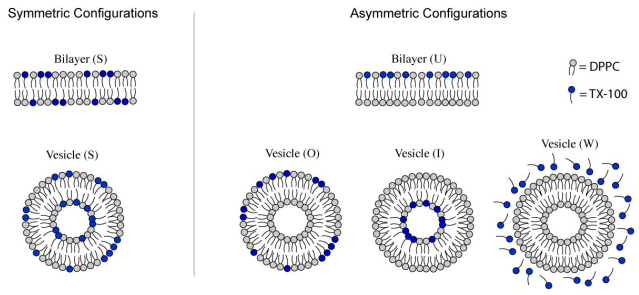

Scheme S1: Snapshots illustrating the initial configurations for symmetric and asymmetric TX-100 distribution in bilayers. The TX-100 molecules are reported in blue. Above each configuration we provide the associated label taken from Table S1.

The starting configuration of the larger vesicle has been accurately built on the basis of that spontaneously obtained in a recent paper by using a hybrid particle-filed approach.[8] In addition, the configuration of the large vesicle was checked against various simulation parameters of DPPC vesicles, both tested by us and present in the literature, such as the ratio of the inner/outer molecules,[9] that in our case is about 0.61 at T = 298 K. Furthermore, the total number of molecules present in the inner and outer layer, respectively, at a given vesicle radius (13.72 nm in our case), has also been tested through the CHARMM-GUI Membrane Builder (http://www.charmm-gui.org/input/membrane), a web-based graphical user interface proposed in ref.[10] for building vesicles composed of different lipids. Part of the DPPC molecules were then randomly substituted with TX-100 units in both layers, obtaining a TX-100/DPPC ratio of 0.43. The vesicle so created is composed of 668 TX-100 and 1528 DPPC molecules in the inner layer, while 1077 TX-100 and 2527 DPPC molecules are present in the outer layer.

In Figure S3 the time behaviour of the repartition of Triton X-100 in the inner and in the outer layers is reported as function of the TX-100/DPPC ratio. As can be seen in Figure S3, in the larger vesicle the distribution of Triton X-100 on both layers become asymmetric, with an average TX-100/DPPC ratio (R = 0.45 ± 0.018) in the outer layer, denoting stability during the simulation and the preference of TX-100 to reach the outer layer.

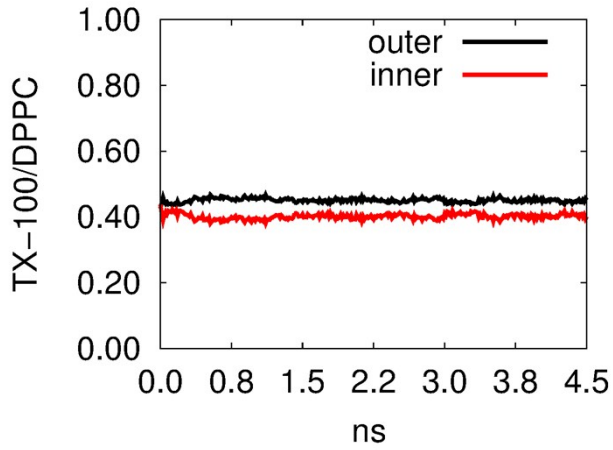

Figure S3: Time behaviour of the TX-100/DPPC ratio, both in the inner and in the outer layers, as function of simulation time.

Comparison between Particle-Particle (PP) and Particle-Field (PF) Coarse Grained Models.

In this section the validation of the interactions between the TX-100 surfactant with a DPPC bilayer is briefly discussed. We will refer to CG models with explicit pair non-bonded interactions as a Particle-Particle model (PP), while the models in which the non-bonded interactions are treated with the MD-SCF approach will be reported as Particle-Field (PF).

The PF CG models of phospholipids have been well validated against the reproduction of several structural properties such as electron density profile and bilayer thickness with respect to experimental data and CG reference models.[11] Moreover, such models have been successfully used to study lipids in non-lamellar phases,[12] lipid bilayers interacting with carbon nanotube bundles,[9] and drug delivery through Pluronic surfactant micelles in DPPC lipid bilayers.[13]

Recently, we developed and validated the PF CG model of TX-100 in a wide range of concentrations in aqueous solutions.[14] In particular, the model reproduces well the experimental critical micellar concentration, shape transition in isotropic micellar phase, and hexagonal order. Here, we compare the electron density profiles of TX-100 in DPPC bilayers at different TX-100 content (molar ratio $R = 0.12$ and 0.43) between the PF and PP models to validate the former against the latter.

We obtain a quantitative agreement between the distributions of TX-100 in DPPC bilayer for the PF and PP models, as reported in Figure S4. In particular, for both TX-100 concentrations ($R = 0.43$ and $R = 0.12$) only small differences are found in the density profiles. The distributions of TX-100 in PF simulations show smoother behaviour with respect to the PP simulations. This expected discrepancy comes from the softer potential describing PF simulations leading to less structured features in the most mobile region of the bilayer. PP and PF simulations produced instead comparable results.

We have also compared the bilayer thickness (DHH), calculated as the distance between the PO_4 distribution peaks, between PF and PP models. In particular, values of DHH = 4.2 ± 0.10 nm for PP and DHH = 4.1± 0.10 nm for PF simulations confirm that the PF CG model is sufficiently accurate to reproduce the results of the reference PP CG simulations.

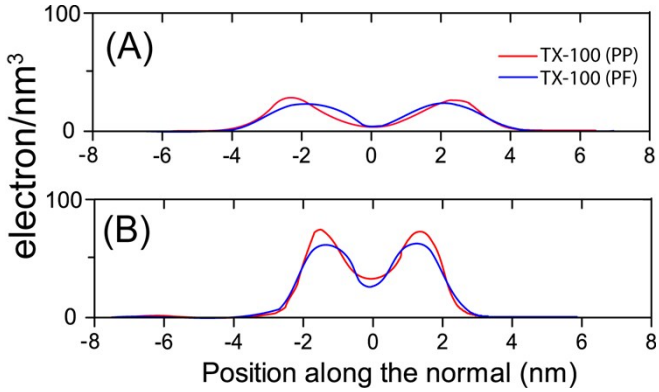

Figure S4: Electron density profiles of TX-100 for PP simulations (red line) and PF simulations (blue line) at two TX-100/DPPC molar ratios *R*: (A) *R* = 0.12, (B) *R* = 0.43. Each profile has been averaged over the last 300 ns of simulation time. The full profiles are reported in Figure S11.

Gyration Radii in the Inertial Frame

In order to measure the asphericity of the mixed TX-100/DPPC vesicles, and to identify prolate and oblate ellipsoidal shapes, we calculated the gyration radius components $RgX,\ RgY,\ RgZ$ in the inertial frame by the following equations:

$$RgX = \sqrt{\frac{\sum_{i=1,N} m_i {x_i}^2}{\sum_{i=1,N} m_i}}, \quad RgY = \sqrt{\frac{\sum_{i=1,N} m_i {y_i}^2}{\sum_{i=1,N} m_i}}, \quad RgZ = \sqrt{\frac{\sum_{i=1,N} m_i {z_i}^2}{\sum_{i=1,N} m_i}}$$

Where $r_i = (x_i, y_i, z_i)$ is the vector between the atom i and the centre of a vesicle, while m_i is the mass of the atom i.

The vesicle axes of inertia (X, Y, Z) are obtained from the diagonalization of the inertia tensor:

$$I = \begin{bmatrix} Ixx & Ixy & Ixz \\ Iyx & Iyy & Iyz \\ Izx & Izy & Izz \end{bmatrix}$$

where:

$$Ixx = \sum_{i=1,N} \left(y_i^2 + z_i^2\right) m_i$$

$$Iyy = \sum_{i=1,N} \left(x_i^2 + z_i^2\right) m_i$$

$$Izz = \sum_{i=1,N} \left(x_i^2 + y_i^2\right) m_i$$

$$Ixy = Iyx = -\sum_{i=1,N} x_i y_i m_i$$

$$Iyz = Izy = -\sum_{i=1,N} y_i z_i m_i$$

$$Izx = Ixz = -\sum_{i=1,N} x_i z_i m_i$$

For all frames of a trajectory the gyration radii are calculated and the vesicle is reoriented to keep the longest gyration radius component coincident with the X direction of the coordinates system (with origin in the c.o.m. of the vesicle).

The size and the shape of mixed TX-100/DPPC vesicle change along the simulation time. In particularly, we have found a strong deformation in vesicle regions enriched in TX-100. Criteria are needed to count a TX-100 molecule to be in a vesicle or in the water phase, to correctly calculate the gyration radii, and also to ascertain the orientation and the position of TX-100 molecules in the outer or inner layer.

To this aim, we have chosen geometrical criteria in which a TX-100 molecule is counted to be part of the vesicle if the beads of the headgroup (types C1, SC1) are included in a certain cut-off distance from the c.o.m. of the vesicle. Starting from the gyration radius calculated at step-1, the TX-100 molecules are counted according to the described criteria and the new gyration radius RgK is calculated. On the basis of the new gyration radius, a second counting is done. The process is iterated until the number of TX-100 counted in the vesicle is constant. As can be seen from Figure S5, in a maximum of 5 iterations the convergence of the TX-100 count is obtained.

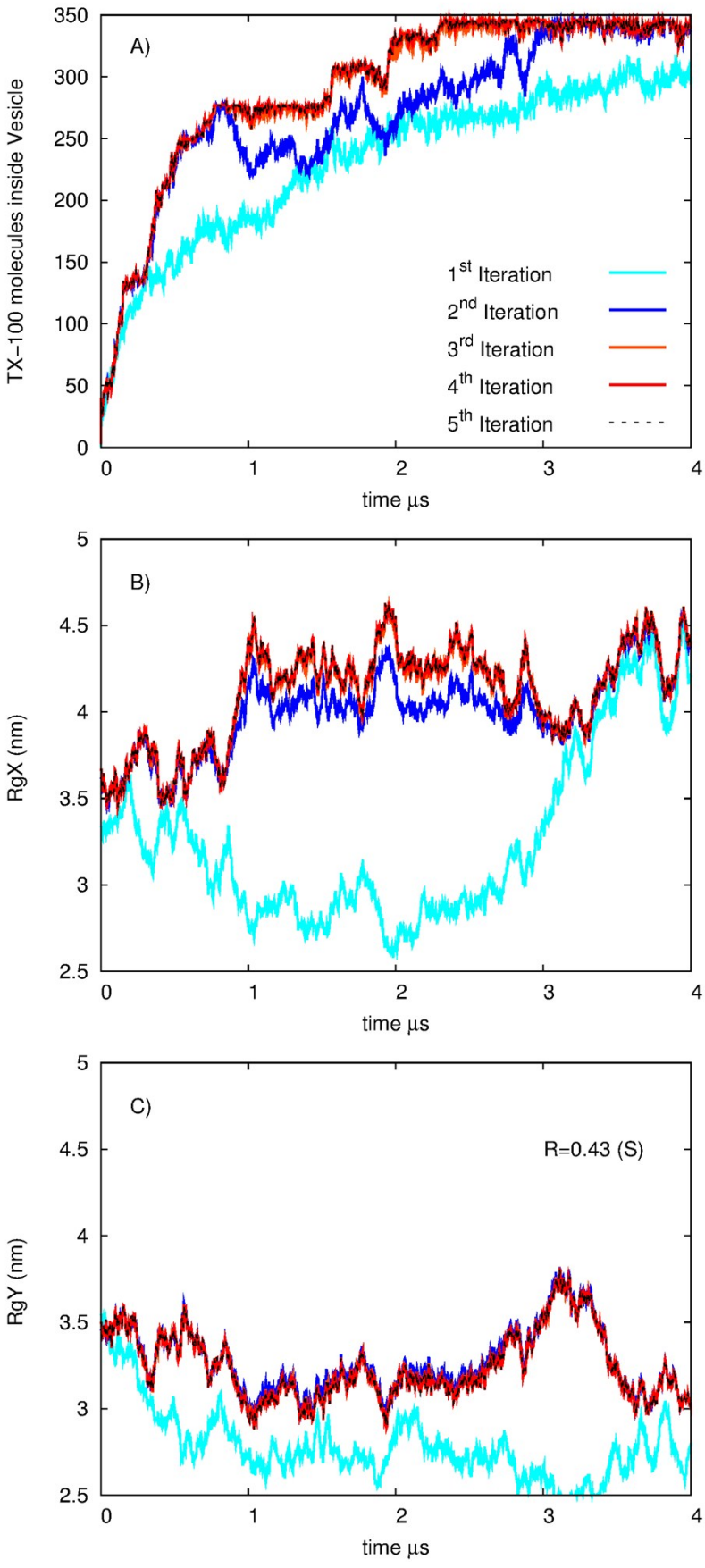

Figure S5: Time behaviour of TX-100 molecules inside the vesicle (A) through various iterations and their respective Rg (RgX,B and RgY,C).

Pure DPPC Vesicle

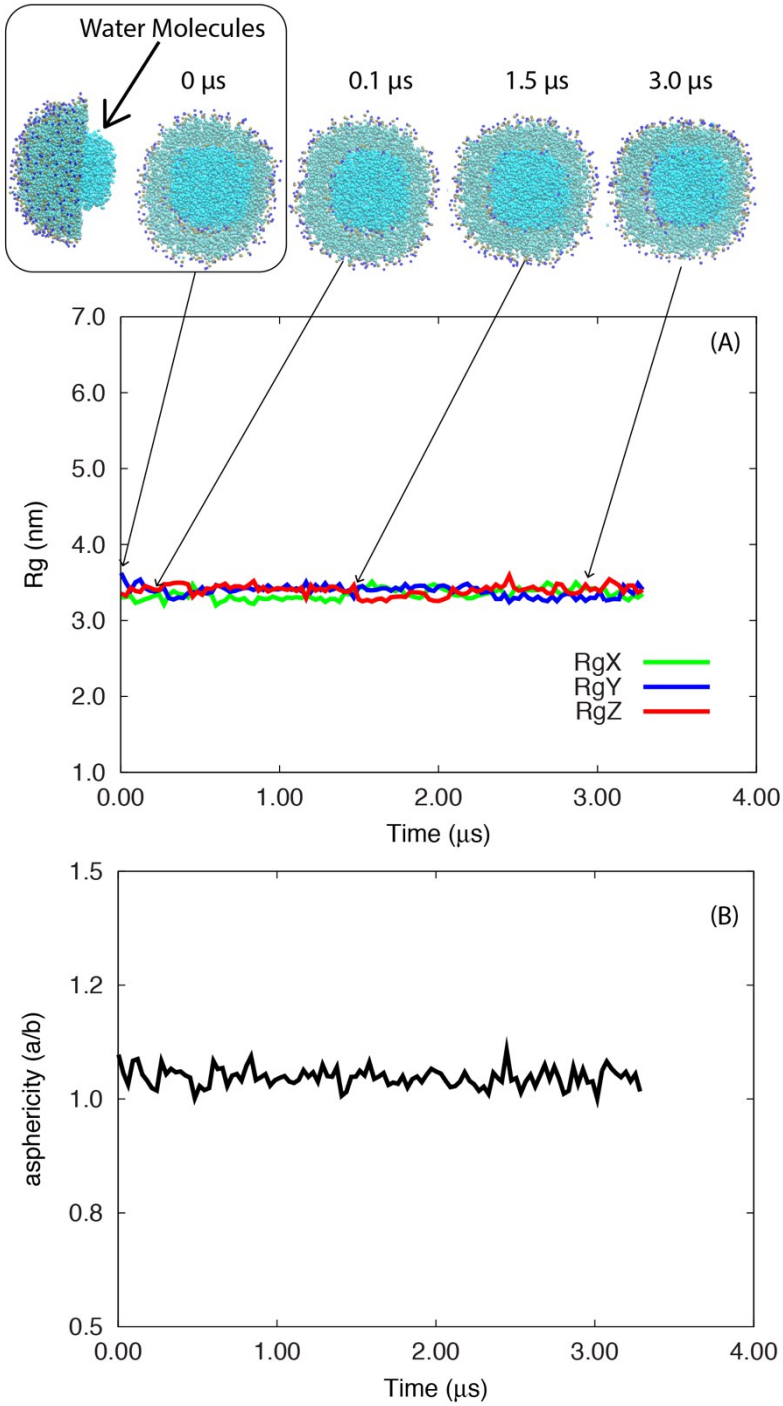

Figure S6: (A) Time behaviour of Rg components of pure DPPC vesicles. On the top of the plot are reported snapshots of vesicle structure with water molecules (in light blue) inside the vesicle cavity, at different simulation times. (B) time behaviour of the asphericity (r_{max}/r_{min}) calculated for pure DPPC vesicles.

Additional Plots

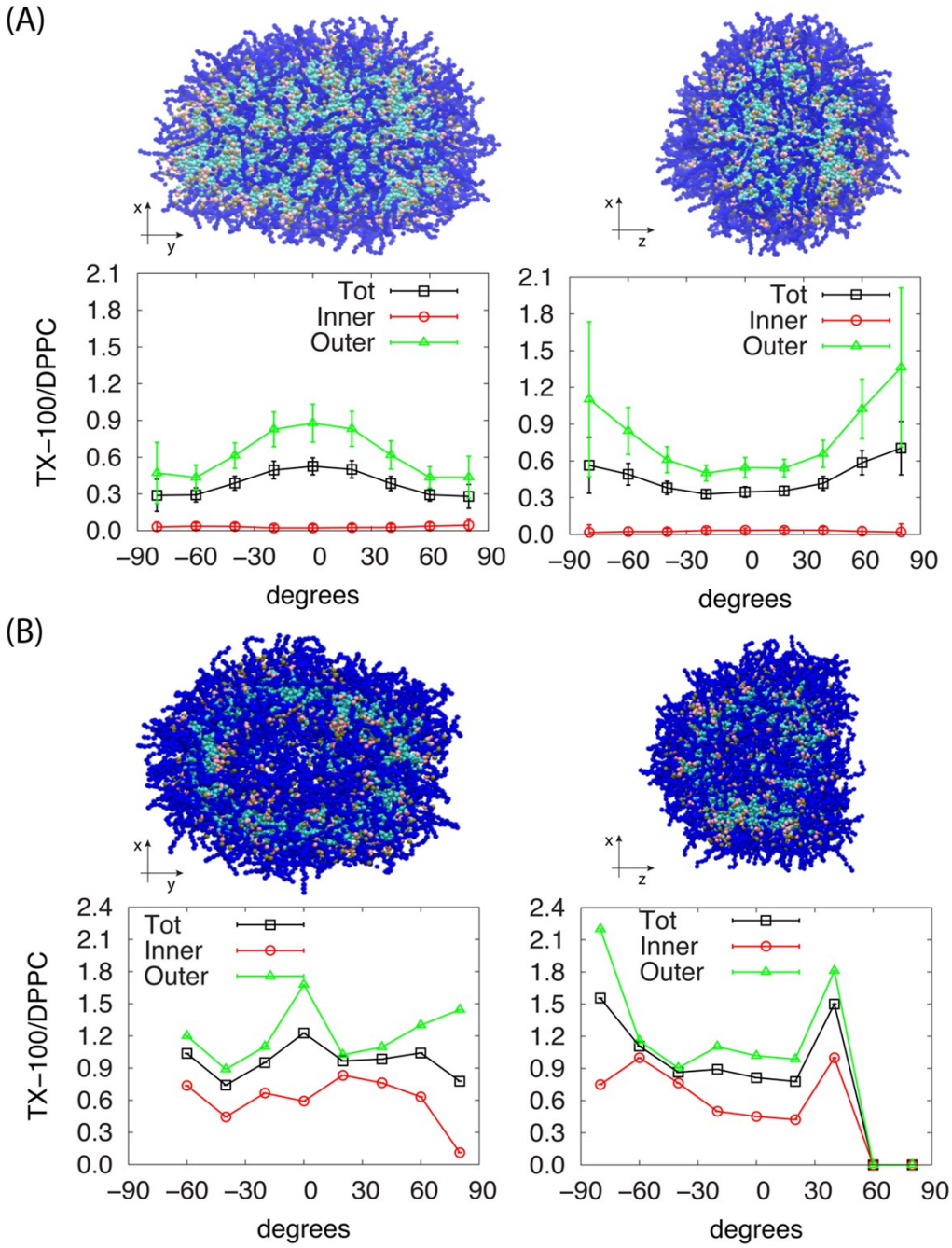

Figure S7: Distribution of TX-100 molecules inside a vesicle for two different orientations: (A) at ratio *R* = 0.43, (B) at *R* = 1.0. On top of each distribution plot a snapshot of the corresponding vesicle structure is reported. The TX-100 molecules are coloured dark blue.

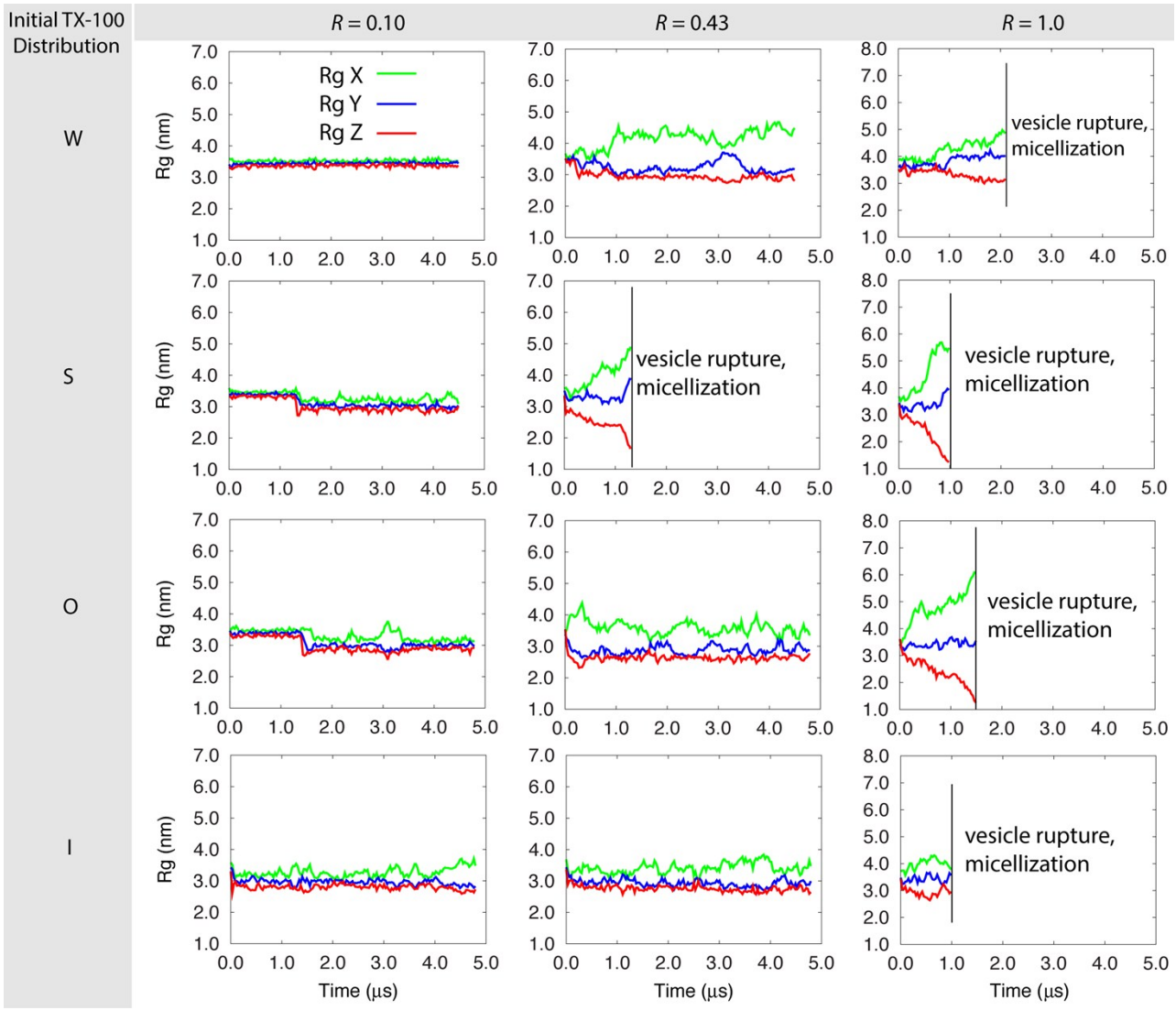

Figure S8: Time behaviour of *Rg* components for different initial TX-100 distributions and different *R* ratios.

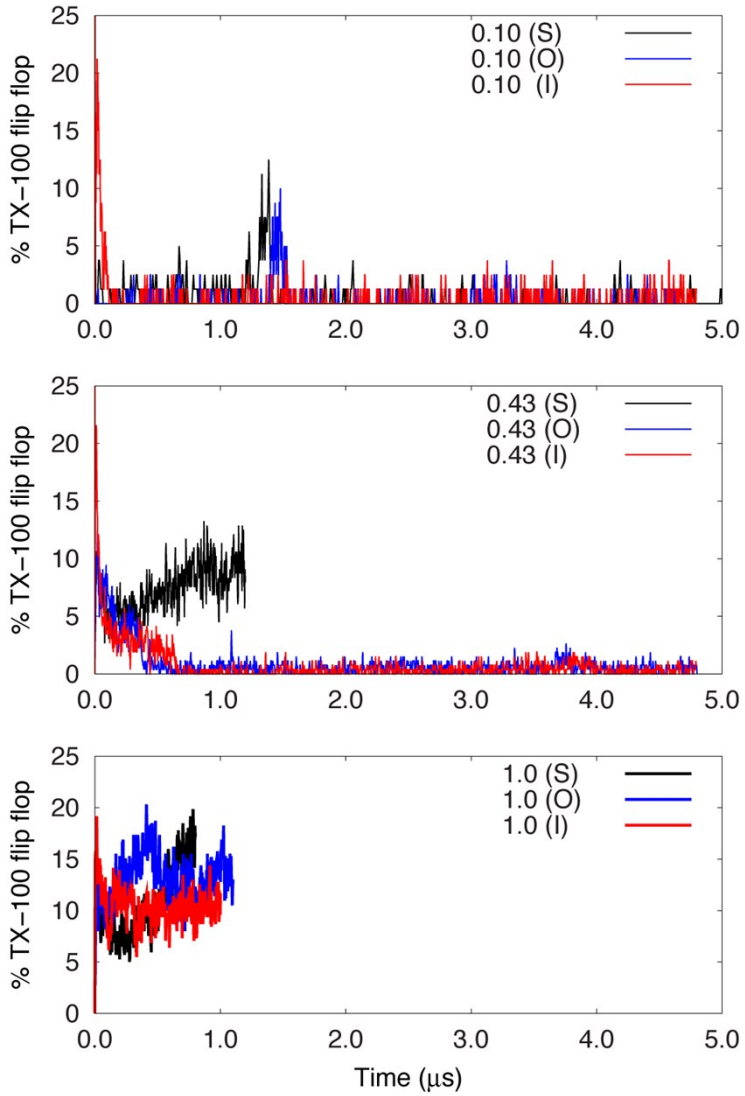

Figure S9: Time behaviour of the percentage of TX-100 molecules involved in flip-flop events, as function of the TX-100/DPPC ratio *R* and for different configurations (S, O, I).

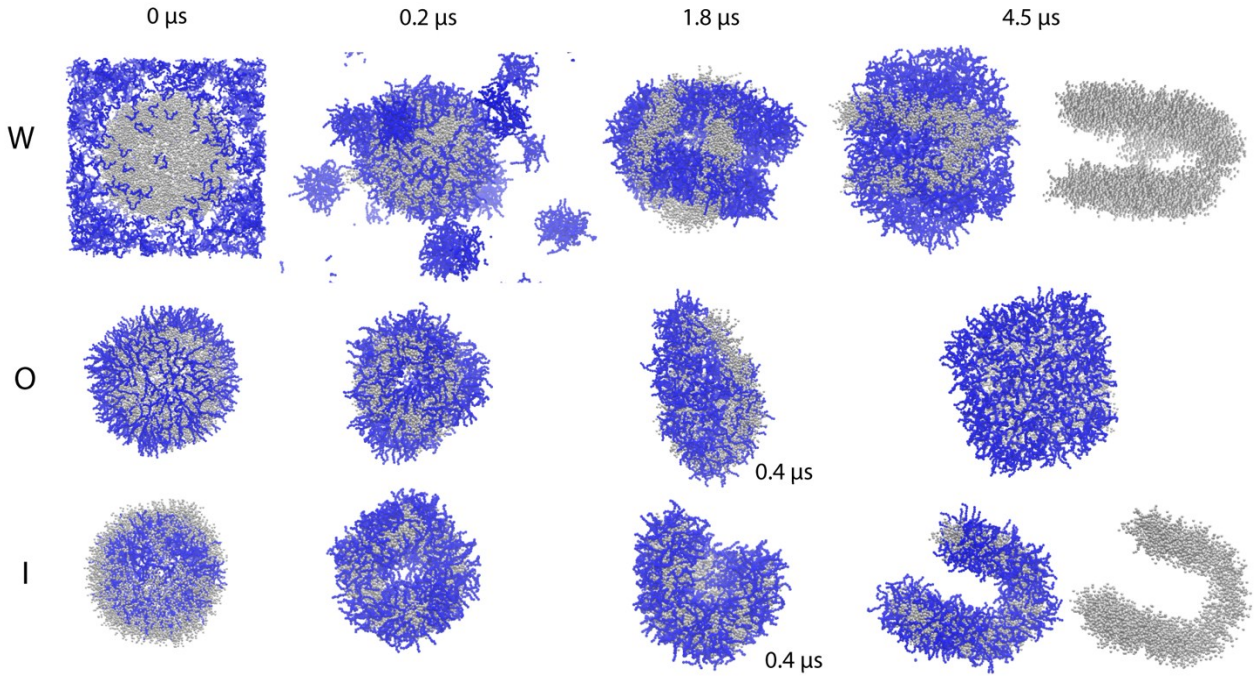

Figure S10: Snapshots of vesicle disruption for a ratio *R* = 1.0 and for different configurations (W, O, I). Blue, TX-100 molecules; grey, DPPC lipids.

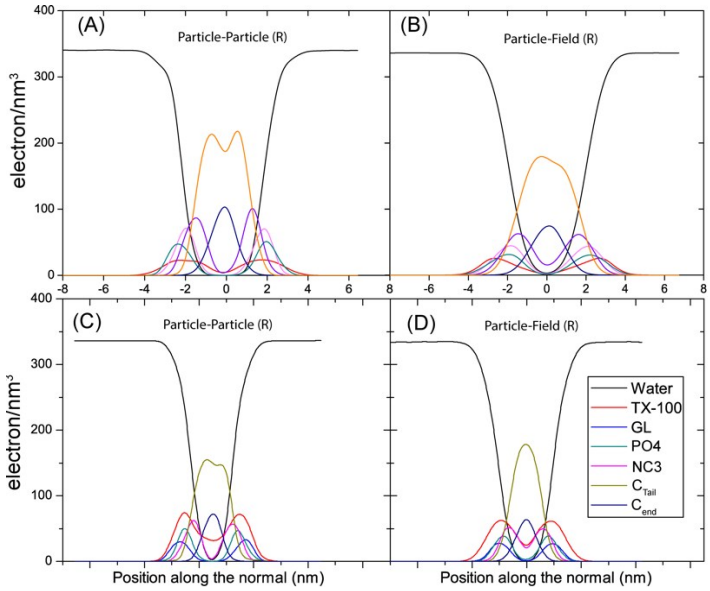

Figure S11: Electron density profiles using PP (A,C) and PF (B,D) simulations for TX-100/DPPC ratios R = 0.12 (A,B) and R = 0.43 (C,D). Each profile has been averaged over the last 300 ns of simulation time.

References:

1. S. J. Marrink, A. H. de Vries and A. E. Mark, *The Journal of Physical Chemistry B*, **2004**, 108, 750-760.
2. Hari S. Muddana, Homer H. Chiang and Peter J. Butler, *Biophysical. Journal.,* **2012**, 102, 489-497.
3 .A. Pizzirusso, A. De Nicola and G. Milano, *The Journal of Physical Chemistry B*, **2016**, 120, 3821-3832.
4 E. Schnitzer, D. Lichtenberg and M. M. Kozlov, *Chemistry and Physics of Lipids,* **2003**, 126, 55-76
5. H. Ahyayauch, M. I. Collado, A. Alonso and Felix M. Goñi, *Biophysical. Journal*., **2012**, 102, 2510-2516.
6 F. M. Goni, M.-A. Urbaneja, J. L. R. Arrondo, A. Alonso, A. A. Durrani and D. Chapman, *European Journal of Biochemistry*, **1986,** 160, 659-665.
7. D. Lichtenberg, H. Ahyayauch and Félix M. Goñi, *Biophysical. Journal.*, **2013**, 105, 289-299.
8. G: J: A. Sevink, F. Schmid, T. Kawakatsu and G. Milano, *Soft Matter,* **2017**, 13, 1594-1623
9. H. J. Risselada and S. J. Marrink, *Physical Chemistry Chemical Physics*, **2009**, 11, 2056-2067
10. S. Jo,Joseph B. Lim, J. B. Klauda, and W. Im, *Biophysical. Journal*. **2009**, 97, 50–58
11. A. De Nicola, Y. Zhao, T. Kawakatsu, D. Roccatano and G. Milano, *Journal of Chemical Theory and Computation*, **2011**, 7, 2947-2962.
12. A. De Nicola, Y. Zhao, T. Kawakatsu, D. Roccatano and G. Milano, *Theoretical Chemistry Accounts*, **2012**, 131, 1-16.
13. A. De Nicola, S. Hezaveh, Y. Zhao, T. Kawakatsu, D. Roccatano and G. Milano, *Physical Chemistry Chemical Physics*, **2014**, 16, 5093-5105.
14. A. De Nicola, T. Kawakatsu, C. Rosano, M. Celino, M. Rocco and G. Milano, *Journal of Chemical Theory and Computation*, **2015**, 11, 4959-4971.